Journal of Physiology (1991), **440**, *pp.* 325–343
With 11 *figures*
Printed in Great Britain

THE MORPHOLOGY AND ELECTRICAL GEOMETRY OF RAT JAW-ELEVATOR MOTONEURONES

BY JANE A. MOORE AND KWABENA APPENTENG
From the Department of Physiology, University of Leeds, Leeds LS2 9NQ

(*Received 10 October 1990*)

SUMMARY

1. The aim of this work was to quantify both the morphology and electrical geometry of the dendritic trees of jaw-elevator motoneurones. To do this we have made intracellular recordings from identified motoneurones in anaesthetized rats, determined their membrane properties and then filled them with horseradish peroxidase by ionophoretic ejection. Four neurones were subsequently fully reconstructed and the lengths and diameters of all the dendritic segments measured.

2. The mean soma diameter was 25 μm and values of mean dendritic length for individual cells ranged from 514 to 773 μm. Dendrites branched on average 9·1 times to produce 10·2 end-terminations. Dendritic segments could be represented as constant diameter cylinders between branch points. Values of dendritic surface area ranged from 1·08 to 2·52 $\times 10^5$ μm^2 and values of dendritic to total surface area from 98 to 99%.

3. At branch points the ratio of the summed diameters of the daughter dendrites to the $\frac{3}{2}$ power against the parent dendrite to the $\frac{3}{2}$ power was exactly 1·0. Therefore the individual branch points could be collapsed into a single cylinder. Furthermore for an individual dendrite the diameter of this cylinder remained constant with increasing electrical distance from the soma. Thus individual dendrites can be represented electrically as cylinders of constant diameter.

4. However dendrites of a given neurone terminated at different electrical distances from the soma. The equivalent-cylinder diameter of the combined dendritic tree remained constant over the proximal half and then showed a pronounced reduction over the distal half. The reduction in equivalent diameter could be ascribed to the termination of dendrites at differing electrical distances from the soma. Therefore the complete dendritic tree of these motoneurones is best represented as a cylinder over the proximal half of their electrical length but as a cone over the distal half.

INTRODUCTION

Our interest is in delineating the spatial organization of different synaptic inputs onto masticatory motoneurones and an essential pre-requisite for this is quantitative information on the geometry of their dendrites. A knowledge of the dendritic geometry can also be the starting point for attempts to model current flow in these neurones (Rall, 1959, 1962, 1977) and eventually for inferring the location of

MS 8048

synaptic inputs from electrophysiological data (Rall, Burke, Smith, Nelson & Frank, 1967; Jack & Redman, 1971*a*, *b*; Redman & Walmsley, 1983; for review see Jack, 1979).

To date there have been no descriptions of the electrical geometry of masticatory motoneurones though there has been one qualitative description of their morphology (Yoshida, Tsuru, Mitsuhiro, Otani & Shigenaga, 1987) and one quantitative assessment of the membrane and firing characteristics of elevator motoneurones (Moore & Appenteng, 1990). We therefore set out to obtain quantitative descriptions of both the general morphology and electrical geometry of jaw-elevator motoneurones by combining the intracellular labelling of identified motoneurones with the determination of their membrane properties. The approach is similar to that used in the determination of the electrical geometry of a variety of different neurones: motoneurones (Ulfhake & Kellerth, 1981; Fleshman, Segev & Burke, 1988; Clements & Redman, 1989), hippocampal (Turner & Schwartzkroin, 1980, 1983), visual cortical (Blakemore, Jack, Larkman & Mason, 1987), lateral geniculate (Bloomfield, Hamos & Sherman, 1987) and superior collicular (Schierwagen & Grantyn, 1986).

The reports on motoneurones have with one recent exception (Bras, Gogan & Tyc-Dumont, 1987) dealt with spinal motoneurones (Ulfhake & Kellerth, 1981, 1983; Egger & Egger, 1982; Cameron, Averill & Berger, 1985; Rose, Keirstead & Vanner, 1985; Cullheim, Fleshman, Glen & Burke, 1987) and so the general question remains as to how far their neuronal geometry is representative of other motoneurone types. In this paper we describe the electrical geometry of elevator motoneurones and then compare this to the geometry of other motoneurones. A summary of the main findings has been communicated to The Physiological Society (Appenteng & Moore, 1988).

METHODS

The surgical preparation and recording set-up were as described by Moore & Appenteng (1990). In brief, rats were initially anaesthetized with a mixture of halothane in oxygen and subsequent anaesthesia maintained with I.V. infusions of pentobarbitone (initial dose = 60 mg kg^{-1}). The masseter nerve was exposed for electrical stimulation, the trachea cannulated and a femoral arterial catheter inserted for monitoring blood pressure. Animals were paralysed with gallamine triethiodide and artificially ventilated for the duration of the experiment. Animals were maintained deeply anaesthetized throughout all stages of the experiment and the criterion used to assess this was that a noxious paw-pinch should elicit no change in blood pressure. A bilateral pneumothorax was performed and end-tidal carbon dioxide levels monitored.

Electrodes

These were pulled from thin-walled glass (o.d. = 1·2 mm, i.d. = 0·94 mm) and filled with a solution of 4% horseradish peroxidase (HRP; Sigma type VI) in 0·5 M-KCl. Their initial tip resistances varied from 20–60 MΩ and were then bevelled down ideally to resistances of between 14 and 18 MΩ. Electrodes were only accepted for use if they could pass at least 10 nA of current in both the hyperpolarizing and depolarizing directions without rectification.

Recording

Masseter and masseter synergist motoneurones were identified as described earlier (Appenteng, Donga & Williams (1985)) and the different responses of the two to electrical stimulation of the masseter nerve are illustrated in Fig. 1*A* and *B*. Following penetration cells were left to stabilize for some 5 min before their membrane properties were determined. The neuronal input resistance (R_n) and membrane time constant (τ_o) were obtained from the transmembrane voltage response to

a 50 ms hyperpolarizing current pulse. The amplitude of these pulses was 0·5–1·0 nA and the voltage responses elicited were within the linear portion of the current–voltage relationship of jaw-elevator motoneurones (Moore & Appenteng, 1990). Between 32 and 104 cycles of current injection were averaged. R_n was calculated from the peak transmembrane voltage response and τ_0 from a plot of the natural log of the decay of the transmembrane voltage against time (Fig. 1*C*). Rheobase was determined from the response to a 50 ms depolarizing current pulse.

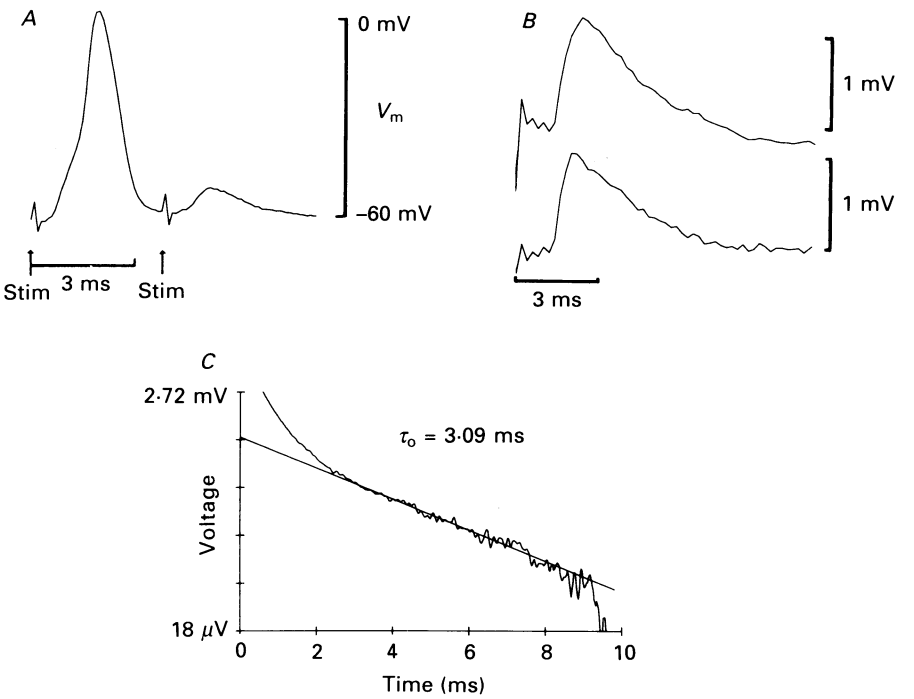

Fig. 1. Antidromic activation of a masseter motoneurone (*A*) and monosynaptic activation of a masseter synergist motoneurone (*B*) following electrical stimulation of the masseter nerve. In *A* the first stimulus elicits an IS-SD spike and the second an M spike. *B*, EPSP (average of 8 sweeps) recorded before (top trace) and after (bottom trace) injecting HRP for 70 min. Note the virtually identical amplitudes. *C*, calculation of membrane time constant for neurone in *B* from a semi-log plot of transmembrane voltage response to a 0·5 nA, 50 ms hyperpolarizing current. *A*, cell 49; *B* and *C*, cell 33.

HRP injection

HRP was injected by passing depolarizing current pulses of intensity 1–4 nA for 10–80 min, using an 80% duty cycle (1·2 s cycle time). By using such relatively low currents the electrodes remained stable throughout the period of injection as judged by the voltage response to the current pulse. Injections were continued as long as the membrane potential was greater than −40 mV. After completing an injection the electrode was left in the cell for a further 5–10 min before it was withdrawn. The bridge balance point was rechecked when the electrode was extracellular and invariably found not to have been altered by the prolonged period of current injection.

Histology

Animals were then maintained alive for a further 60–90 min (3 h in one case; cell 27) to allow the HRP to diffuse throughout the neurone. Heparin (2500 units I.V.) was given some 10 min prior to perfusing the animals first with a Tyrode mixture and then 500 ml of a chilled 1·75%

glutaraldehyde–0·5% paraformaldehyde fixative, and finally 500 ml of chilled 10% sucrose solution. The brain was then removed and allowed to sink in a 30% sucrose solution. The fixative and sucrose solutions were made up in 0·1 M phosphate buffer (pH = 7·4). Frozen, serial, transverse sections (60 μm) were cut and the tissue processed for HRP activity using the tetramethylbenzidine (TMB) method of Mesulam (1982). We chose to use the TMB method because of its particularly high sensitivity but the potential pitfalls are that the reaction product may extend outside neuronal processes and the background staining may be high (Mesulam, 1982). Both problems stem from inadequate control of the reaction sensitivity. We used a staining solution that contained (per litre) 0·06 ml of hydrogen peroxide, 1 g of sodium nitroprusside and 5 mg of TMB (Appenteng & Girdlestone, 1987). Sections were mounted onto chrome alum slides and air-dried for at least 10 days before they were dehydrated in butanol (Jankowska, 1985).

Neuronal reconstructions and morphometric measurements

Initially a low-power (× 100) reconstruction of the neuronal morphology was made from camera lucida drawings to allow the location and orientation of the neurone to be determined and then subsequently a more detailed high-power reconstruction (× 1060) was made. Measurements of the minimum and maximum soma diameter and length and diameter of dendrites were made from these large scale reconstructions using a digitizing tablet (resolution = 0·01 mm). The diameters of all dendrites were usually measured at intervals of 5–10 μm and never at more than 20 μm. We used a pythagorean correction to correct all measurements of length for the effect of depth through the sections. No correction was made for shrinkage induced by the histological procedures.

Morphometric calculations

Soma surface area. This was derived by approximating the soma to an ellipsoid.

Dendritic surface area. Dendritic segments (here defined as the distance between two consecutive branch points along the same dendrite) were approximated as cylinders and their areas summed to give the complete dendritic surface area.

Branch point ratio. Rall (1959) has shown that impedance matching occurs at branch points when the summed diameters of daughter dendrites (d_{daughter}) raised to the $\frac{3}{2}$ power equals the diameter of the parent dendrite (D_p) raised to the $\frac{3}{2}$ power (i.e. $\Sigma(d_{\text{daughter}}^{\frac{3}{2}}) = D_p^{\frac{3}{2}}$).

Tapering of dendrites. The amount of tapering with increasing electrical distance from the soma, within individual dendrites and throughout the complete dendritic tree was assessed by the argument below which is broadly similar to that employed by Clements & Redman (1989). However, one important difference is that Clements and Redman's arguments required a knowledge of both the electrical properties and morphology of cells whereas ours simply requires a knowledge of the morphology of neurones.

Considering first the case of an individual dendrite of a neurone, the condition required for impedance matching to occur throughout the dendrite is that the diameter of the primary dendrite (defined as the segment of dendrite extending from the soma to the first point of branching of the dendrite) should equal the diameter of all the other segments of the dendrite raised to the $\frac{3}{2}$ power summed and raised to the $\frac{2}{3}$ power:

$$D_x = (\Sigma(d_n^{\frac{3}{2}}))^{\frac{2}{3}}, \tag{1}$$

where d_n is the diameter of any dendritic segment. The right hand-side of the equation was used to calculate the diameter of the dendrite at any point in the dendritic tree and the answer obtained for the left-hand side (D_x) will be referred to from here on as the equivalent diameter of an individual dendrite. Where the combined diameter of the other dendritic segments is less than D_x then electrically there is tapering of the dendrite with distance from the soma, and where it is greater than D_x there is flaring of the dendrite with electrical distance from the soma.

The electrical distance from the soma to any point along a dendrite can be determined by calculation of the electrotonic length (L) which in turn can be derived starting from the relationship:

$$L = l/\lambda, \tag{2}$$

where l = physical length of dendritic segment and λ = the space constant. The value of L to a point in the dendritic tree is simply the sum of the individual values obtained for segments lying along the path from the soma to the point in question. λ can be approximated as:

$$\lambda = l \times \sqrt{(k\,d)}, \tag{3}$$

where k (a constant) $= R_m/4R_i$ and d = diameter of dendritic segment. R_m (specific membrane resistivity) and R_i (specific cytoplasmic resistivity) are assumed to be constant throughout the neurone. Equation (3) allows the electrical distances along dendrites to be approximated purely from morphological data and describes the effect of diameter on the electrotonic length. From eqn (3) it can be seen that the primary dendrite will have the longest space constant as its diameter is greatest. Continuing out along the dendritic tree, the space constant will decrease and electrotonic length of the dendrite will increase in proportion to the square root decrease in the diameter of dendritic segments.

TABLE 1. Values for equivalent length and diameter

Dendrite	Physical diameter	Physical length	$d^{\frac{3}{2}}$ ($\mu m^{\frac{3}{2}}$)	Equivalent length (μm)
$d_{2\cdot1}$	4	100	8	$100 \times \sqrt{(7\cdot94/4)} = 140\cdot89$
$d_{2\cdot2}$	1	100	1	$100 \times \sqrt{(7\cdot94/1)} = 281\cdot78$

TABLE 2. Values for equivalent length and diameter including two new branches

Dendrite	Physical diameter	Physical length	$d^{\frac{3}{2}}$ ($\mu m^{\frac{3}{2}}$)	Equivalent length (μm)
$d_{2\cdot2}$	1	100	1	$281\cdot78 - 140\cdot89 = 140\cdot89$
$d_{3\cdot1}$	1	100	1	$100 \times \sqrt{(7\cdot94/1)} = 281\cdot78$
$d_{3\cdot2}$	1	50	1	$50 \times \sqrt{(7\cdot94/1)} = 140\cdot89$

TABLE 3. Values for equivalent length and diameter for remaining dendrite

Dendrite	Physical diameter	Physical length	$d^{\frac{3}{2}}$ ($\mu m^{\frac{3}{2}}$)	Equivalent length (μm)
$d_{3\cdot1}$	1	100	1	$281\cdot78 - 140\cdot89 = 140\cdot89$

To calculate the equivalent diameter for the combined dendritic tree of a neurone the equivalent diameter of the nominal primary dendrite ($D_{combined}$) is taken as the diameter of the individual primary dendrites ($d_{primary}$) each raised to the $\frac{3}{2}$ power, summed and raised to the $\frac{2}{3}$ power:

$$D_{combined} = (\Sigma(d_{primary}{}^{\frac{3}{2}})^{\frac{2}{3}}). \quad (4)$$

The equivalent diameter of subsequent dendritic segments is calculated as in eqn (1). The equivalent length of this combined primary dendrite is calculated from:

$$L' = l \times \sqrt{(D_{combined}/d_{primary})}, \quad (5)$$

where L' is referred to as the equivalent length. The equivalent length of subsequent dendritic segments is calculated by substituting d_n for $d_{primary}$ in eqn (5).

For individual dendrites, the equivalent diameter of the nominal primary dendrite ($D_{combined}$) is again used to calculate equivalent length. This is to allow the equivalent length of the different dendrites of a neurone to be compared. The equivalent length of the primary dendritic segment is calculated as in eqn (5) and the equivalent lengths of subsequent dendritic segments calculated by substituting d_n for $d_{primary}$ in eqn (5).

The steps in the calculation of equivalent diameter and length are illustrated for the case of a hypothetical neurone with two dendrites (Fig. 2*A*). The diameter of each of the primary dendrites is 5 μm, thus the diameter of the nominal primary dendrite is $(5^{\frac{3}{2}} + 5^{\frac{3}{2}})^{\frac{2}{3}}$, i.e. 7·94. For the individual dendrite shown in Fig. 2, the equivalent diameter of the primary dendrite is simply taken as its physical diameter and its equivalent length is calculated as 125·99 μm (i.e. $100 \times \sqrt{(7\cdot94/5)}$). The

dendrite then branches in two and the values of equivalent diameter and length are calculated in Table 1.

The equivalent diameter will be 4·33 μm ($(8+1)^{\frac{2}{3}}$) and this will be for a distance of 140·89 at which point dendrite$_{2\cdot1}$ branches to give rise to two daughter branches. The distance of 140·89 μm is subtracted from the equivalent length of dendrite$_{2\cdot2}$ to give the remaining distance for dendrite$_{2\cdot2}$ and the table redrawn to include the two new branches (Table 2).

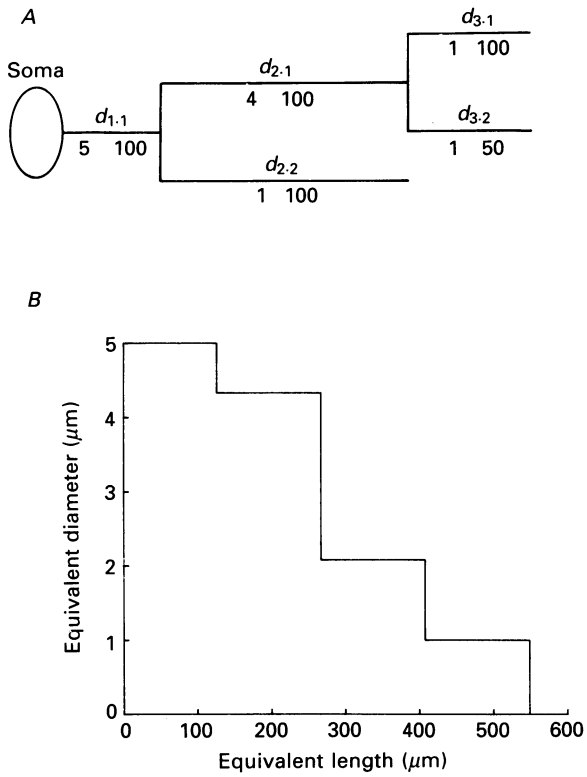

Fig. 2. Determination of the equivalent diameter and length of a single hypothetical dendrite of a neurone. The neurone is assumed to have two dendrites. *A*, branching pattern of the dendrite, second dendrite of the neurone is not shown. The subscripted numbers above each segment show the segment number and the values below each segment show the diameter (on left) and length (on right) of the segment. *B*, plot of equivalent diameter and length values calculated for dendrite (see text for values).

The equivalent diameter of the three branches is 2·08 (i.e. $(1+1+1)^{\frac{2}{3}}$) and this will be for a distance of 140·89 μm at which point both dendrite$_{3\cdot2}$ and dendrite$_{2\cdot2}$ terminate. The length of these dendrites is then subtracted from the remaining dendrite and the table redrawn (Table 3).

The equivalent diameter of the remaining dendrite is 1 and this will be for a distance of 140·89 μm at which point the dendrite terminates. Figure 2*B* shows the plot of equivalent diameter against length for this single dendrite.

Electrotonic length. The electronic length of individual dendrites was calculated from eqn (2) by summing the electrotonic length of the individual dendritic segments stepwise along a common pathway from the soma to the most distal dendritic segment. Membrane capacitance (C_m) was

assumed to be 1 μF cm^{-2} and therefore R_m (Ω cm^2) assumed to equal τ_o (ms). R_i was assumed to equal 100 Ω cm^{-1} (Rall, 1977). The value of L for the entire dendrite was obtained by taking the mean of the individual dendritic terminations.

Input conductance. A cylindrical dendritic segment can be represented by a finite length of core conducting cable (Rall, 1959). The input conductance (G_{in}) of any segment is given by:

$$G_{in} = B_{in} \times d^{\frac{3}{2}} \times \pi/2 \times (R_m \times R_i)^{-\frac{1}{2}} \quad (6)$$

and

$$B_{in} = (B + \tanh(L))/(1 + B \tanh(L)), \quad (7)$$

where B represents the terminating conductance of the segment normalized with respect to the conductance of a semi-infinite cable of the same diameter d. B was taken as either 0 or 1, values assumed for either a sealed end or open-ended cable. At the soma the conductances of all the dendritic trees (G_d) and of the soma (G_s) were added to give the computed neurone input conductance (G_{morph}):

$$G_{morph} = G_s + G_d, \quad (8)$$

where $G_s = A_s/R_m$, where A_s is the soma surface area.

RESULTS

The data here reported are derived from five motoneurones that were filled with HRP. Four were identified as masseter motoneurones and one as a masseter synergist motoneurone. Four cells were completely reconstructed and then further analysed quantitatively as outlined in the Methods. The fifth cell was used only for measurements of soma size and axon morphology as the three tracks made in the motor nucleus prior to penetration of it resulted in a high level of background artifact due to the bleeding induced. The electrical properties of the neurones are summarized in Table 4.

General Morphology

Figure 3 shows reconstructions of the morphology of two neurones and illustrates the general tendency observed for dendritic branching to be more predominant in the dorsal half of the dendritic tree than in the ventral half. What cannot be illustrated in the figure was the tendency for dendritic branches to be also orientated rostrally.

The maximum and minimum diameters of the somata ranged from 35 to 15 μm with the mean diameter for the sample being 25 μm (range = 24–27·8). This figure is identical to the mean value reported for rat elevator motoneurones labelled by intramuscular injections of HRP (Rokx, van Willigen & Juch, 1985). Six to eight dendrites radiated from the somata of each motoneurone in our sample and apart from one dendrite which did not branch, individual dendrites branched between 2 and 33 times in total (225 branch points for the total sample; mean = 9·1 (dendrite)$^{-1}$; S.D. = 2·66). The total number of branches produced by the four cells was 391. Sixty-four per cent of these were fourth order or below and the remainder fifth to ninth order. On average each dendrite gave rise to 10·2 end-terminations (n = 252; S.D. = 2·7).

The maximum lengths of dendrites were determined by summing the lengths of dendritic segments that lay along a path between the soma and the most distal termination. Values of mean dendritic length for individual cells were 544 (S.D. = 116; cell 33), 773 (S.D. = 207; cell 43), 514 (S.D. = 165; cell 37) and 720 μm (S.D. = 120; cell 27). These values should be compared with the dimensions of the motor

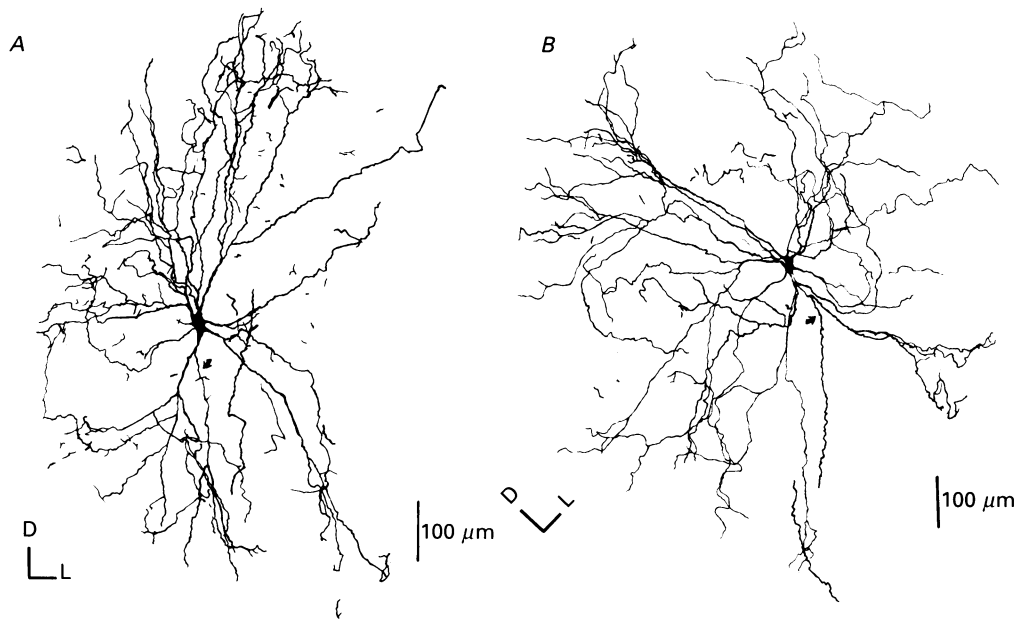

Fig. 3. Reconstructions of the morphology of two neurones. *A*, cell 33; *B*, cell 43. Note the tendency for dendrites to be dorsally directed. Arrowheads identify the axons which in both cases gave off collaterals. D, dorsal; L, lateral.

TABLE 4. Electrical properties of the neurones

Unit no.	V_m (mV)	Input resistance (MΩ)	τ_0 (ms)	Rheobase (nA)	No. of dendrites	Dendritic surface area (μm^2)	Mean soma diameter (μm)	Soma surface area (μm^2)	Total neuronal surface area (μm^2)
27	−60	1·81	—	3·25	6	$2{\cdot}522 \times 10^5$	27·7	$3{\cdot}3 \times 10^3$	$2{\cdot}55 \times 10^5$
33	−75	0·81	3·09	1·38	7	$1{\cdot}817 \times 10^5$	24·0	$2{\cdot}9 \times 10^3$	$1{\cdot}846 \times 10^5$
37	−47	1·98	3·47	4·22	6	$1{\cdot}079 \times 10^5$	24·1	$2{\cdot}5 \times 10^3$	$1{\cdot}104 \times 10^5$
43	−60	4·12	3·43	2·64	8	$2{\cdot}427 \times 10^5$	27·8	$2{\cdot}9 \times 10^3$	$2{\cdot}456 \times 10^5$
49	−60	3·8	2·18	3·30	7	—	25·0	$1{\cdot}9 \times 10^3$	—

nucleus which are approximately 800 μm in length and 500 μm in width: thus on average the dendrites can potentially traverse the full width and almost the entire length of the nucleus.

Quantitative dendritic morphology

Patterns of branching and termination

Figure 4*A* summarizes the pattern of branching of all the neurones by plotting the variation of the mean dendritic segment length calculated for the total sample against dendritic segment number. The figure shows that the primary dendrites are short, the second to fourth order dendritic segments are long and there is then a progressive decrease in length over subsequent segments. Figure 4*B* shows the proportion of dendritic segments (expressed as a percentage of the total number)

which represented end-terminations. Dendritic segments of fifth order and above accounted for 60% of the total number of terminating segments.

Diameters and surface area

Figure 5 shows a typical series of measurements taken along a dendritic segment of a neurone which in common with all bar two dendrites of one neurone in our

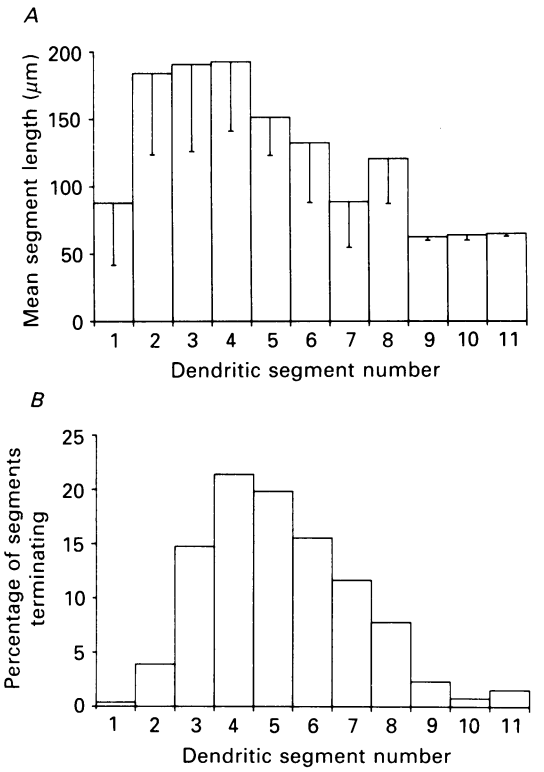

Fig. 4. Representation of the branching pattern of the total sample of neurones. *A*, variation of mean dendritic segment length with segment number. Note the continual decrease in the mean lengths after the fourth order segments. Error bars show standard deviations. *B*, proportion of all segments forming end-terminations in each segment. The total number of end-terminations for the sample was determined and the percentages shown in the plot calculated.

sample (cell 27) showed no dendritic beading. The most striking feature is the great variability in values obtained. However, this is random in nature ($r^2 = 0{\cdot}0$), a feature common to all other segments examined. Two conclusions follow from this: (1) there is no systematic tapering or flaring of dendritic diameter between branch points and (2) the mean of these measurements represents the most reliable estimate of the diameter of the segment and so this was the value used.

A consequence of the above is that the surface area of dendritic segments could be calculated by representing them as cylinders. Values of the combined dendritic surface area for our sample ranged from $1{\cdot}08$ to $2{\cdot}52 \times 10^5$ μm^2 and values of dendritic

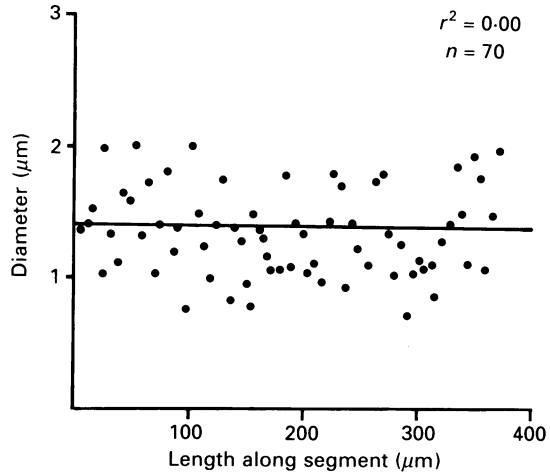

Fig. 5. Variations in diameter along a dendritic segment. The measurements vary essentially randomly over a twofold range. Line shows the mean diameter calculated from the measurements. Mean = 1·39 μm.

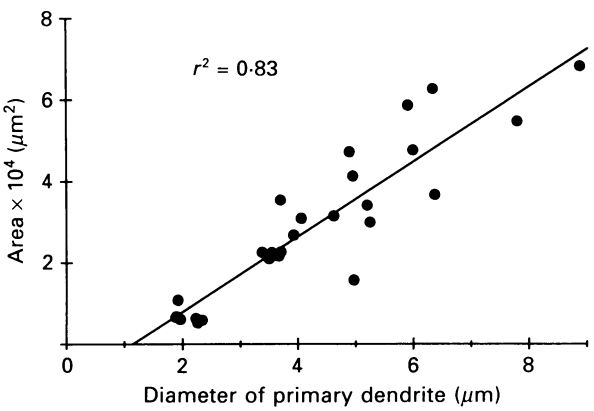

Fig. 6. Relationship between dendritic surface area and diameter of primary dendrites. Solid line is linear least-squared fit to data.

to total surface area from 98 to 99% (see Table 4). The surface area of individual dendrites was linearly related to the diameter of the primary dendrites (Fig. 6; r^2 = 0·83).

The plots in Fig. 7*A* and *C* show the typical variation in dendritic surface area with distance from the soma for two neurones. In each case there is an initial increase in area and then a pronounced reduction over approximately the distal third of the dendritic tree. The increase in area would be expected on the basis of the branch point ratio obtained for these neurones (see below) while the reduction in area in the distal part of the dendritic tree would suggest that many dendrites terminate in this region. Figure 7*B* and *D* shows plots of the cumulative surface area against distance for the same two neurones and serve to emphasize that area increases approximately uniformly and then levels off in the distal third of the dendritic tree.

Electrical geometry of neurones

The large dendritic to soma surface area suggests that the majority of synaptic inputs must be onto the dendritic tree. Therefore the way in which current flows in their dendrites is clearly of importance in understanding the integration of synaptic

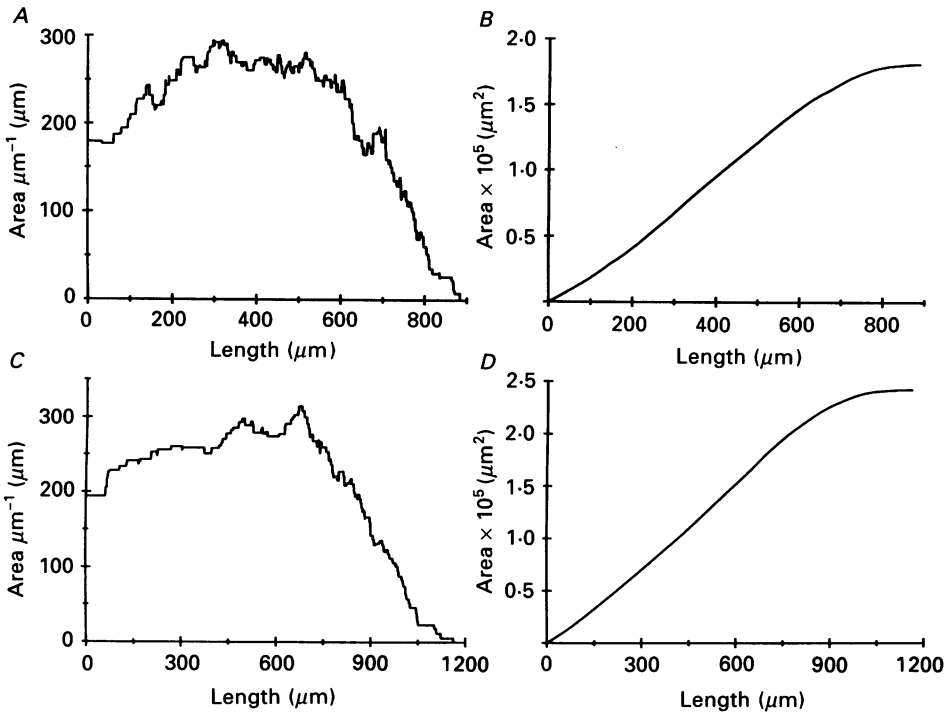

Fig. 7. Variation of dendritic surface area with distance from the soma. *A* and *C* show plots of the surface area μm^{-1} with distance from the soma for two neurones; *B* and *D* show the corresponding variation in their cumulative surface areas. *A* and *B* are from cell 33; *C* and *D* from cell 43.

inputs in these neurones. Current flow through the dendritic tree will in part be determined by its complex branching morphology. This morphology can be simplified in two separate ways: (1) as a single equivalent cylinder or (2) as a series of compartments (Rall, 1959, 1962). The conditions necessary for representing the dendritic tree as a single equivalent cylinder are first that there should be impedance matching at branch points and second that the dendrites must all terminate at the same electrotonic distance from the soma. We have tested for these two conditions below.

Impedance matching

This occurs at branch points when the ratio $d_{daughter}^{\frac{3}{2}}/D_p^{\frac{3}{2}} = 1$ (Rall, 1959). The significance of this is that where this occurs the three branches can be collapsed into a single cylinder. Figure 8*A* shows the distribution of this ratio for all our cells. The

values range from 0·8 to 1·19 with a mean of 1·00 (n = 185; S.D. = 0·06). Figure 8B shows a plot of this ratio against the diameter of the parent dendrite and shows that there is no systematic variation in this ratio across the dendritic tree.

Termination of dendrites

As there is impedance matching at individual branch points it is possible to represent the entire dendritic tree as an equivalent cylinder of constant diameter if

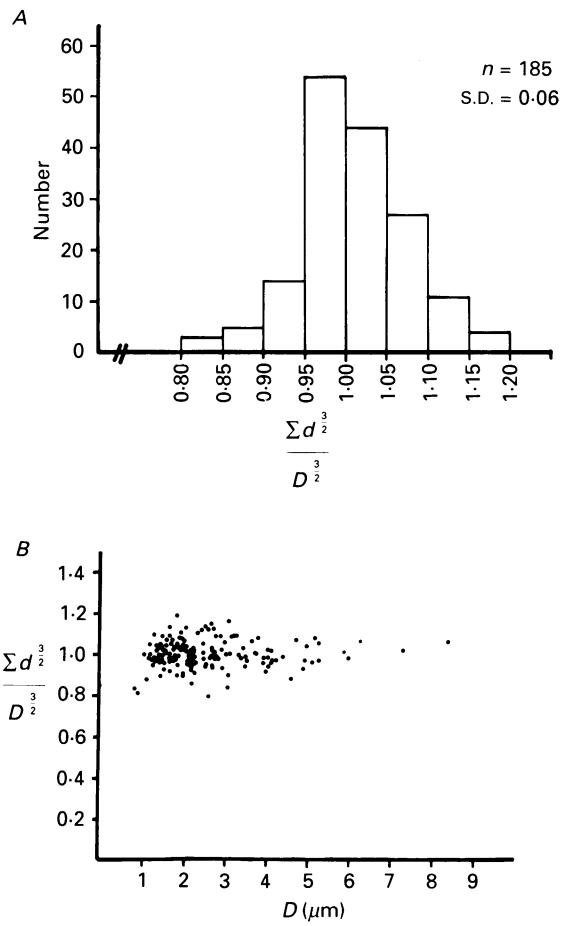

Fig. 8. Branch point ratios for all units. A, histogram of ratios; mean = 1·00. B, ratios plotted against diameter of parent dendrite. Clearly impedance matching occurs at branch points throughout the dendritic tree.

in addition eqn (1) (see Methods) is satisfied throughout the dendritic tree. The alternatives are either that the diameter of the dendritic tree decreases with electrical distance from the soma (tapers) or that it increases (flares).

Figure 9 shows the variation in equivalent diameter with increasing electrical

distance from the soma of all the individual dendrites of a cell. The figure serves to emphasise two features. First the diameter of most individual dendrites can be seen to remain relatively constant throughout most of the equivalent length of the dendrites. Therefore to a first approximation the individual dendrites can be

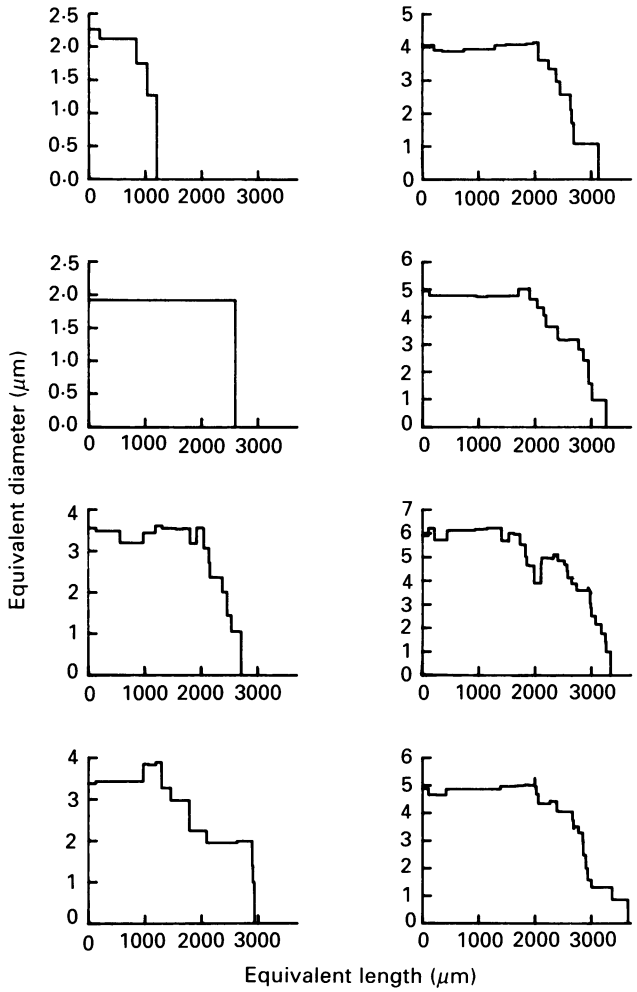

Fig. 9. Variation in equivalent diameter of the individual dendrites of a neurone (cell 43) with equivalent length from the soma. Diameter remains approximately constant and then reduces abruptly in the most distal part of the dendrites. Note that dendrites terminate at widely differing equivalent lengths.

represented electrically as equivalent to cylindrical cables of constant diameter. Second the individual dendrites terminate at differing electrical lengths from the soma. For example the shortest dendrite terminates at an equivalent length of 1205 μm while the longest dendrite terminates at 3655 μm.

Figure 10*A* and 10*B* shows plots of equivalent diameter against equivalent length

for the combined dendritic tree of two neurones with the neurone in Fig. 10*A* being the same as the one shown in Fig. 9. In each case the diameter remains constant for approximately 50% of the total equivalent length of the neurone and then tapers rapidly over the distal half of the equivalent length of the neurone (Fig. 10*A* and *B*).

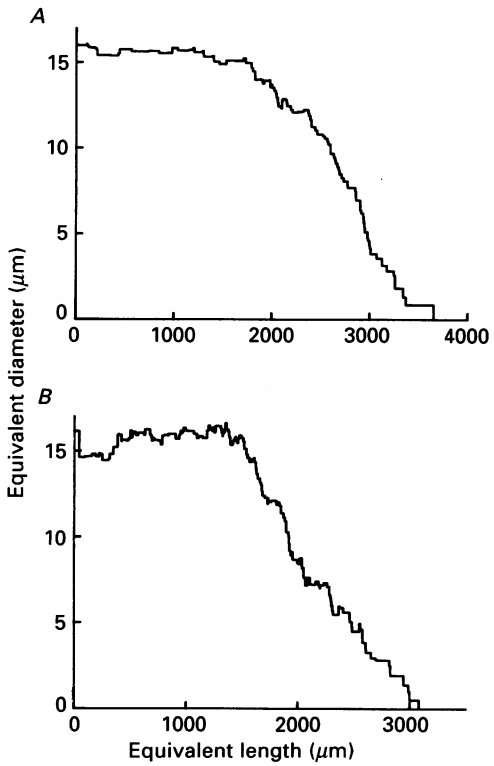

Fig. 10. Variation in the equivalent diameter of the combined dendritic tree of two neurones with equivalent length from the soma. Note that in each case diameter remains approximately constant over the proximal half of the dendritic tree and then decreases abruptly in the distal half. *A*, cell 43; *B*, cell 27.

Precisely the same trends were shown by the remaining two neurones in our sample so suggesting that this may be a characteristic feature of elevator motoneurones. In each case the tapering over the distal half of the equivalent length could be ascribed to the termination of individual dendrites at different electrical distances from the soma (cf. Figs 9 and 10*A*).

Electrotonic length

A more conventional estimate of the electrical length of dendrites is the electrotonic length (L) and Fig. 11 shows the distribution of values calculated for all the individual dendrites of the three neurones for which values of τ_0 were obtained. A significant feature of the plots is the wide variations evident in values of L for the different dendrites of a neurone. The differences in values between neurones are in

part dependent on errors in the estimation of τ_0 because R_m is estimated in this calculation by assuming that $\tau_0 \propto R_m$. However, the variation within a neurone is independent of this error.

The membrane time constant will be underestimated if there is a leak at the soma because of the increased conductance there. One way of assessing if there is a leak is

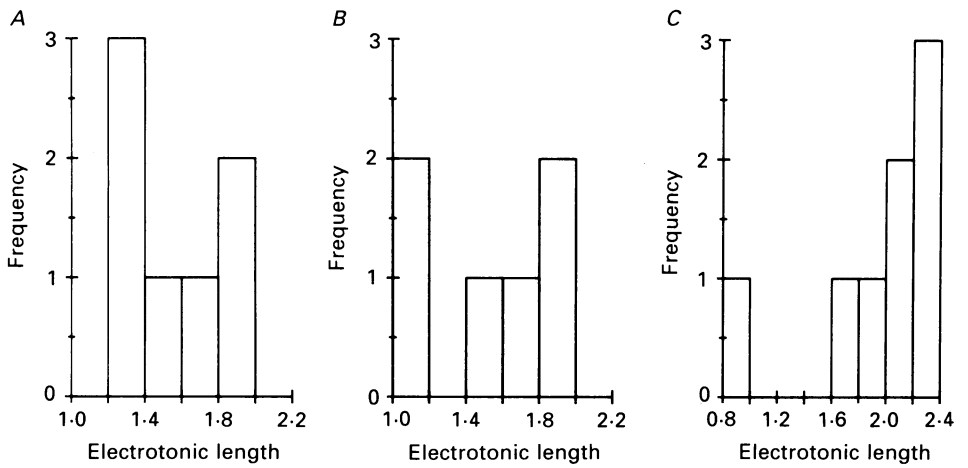

Fig. 11. Plot of the distribution of mean electrotonic lengths of the individual dendrites of the three neurones for which time constants were obtained. *A*, cell 33 (mean = 1·54); *B*, cell 37 (mean = 1·49); *C*, cell 43 (mean = 1·95).

to compare the input conductance derived from the morphological data with the value obtained from the input resistance of the neurone (G_{in}).

Given that the individual dendrites can be approximated as cylinders of constant diameter over most of their length, then the input conductance of a dendrite can be calculated using the derived value of L and the diameter of the primary dendrite (see eqns (6) and (8) in Methods). The whole cell input conductance calculated from the morphological data (G_{morph}) was in all cases smaller than the value obtained from the input resistance. Values of G_{morph} were $1{\cdot}19 \times 10^{-7}$ (cell 37), $1{\cdot}92 \times 10^{-7}$ (cell 33), $1{\cdot}83 \times 10^{-7}$ S (cell 43). The respective values of G_{in} were $5{\cdot}05 \times 10^{-7}$, $12{\cdot}4 \times 10^{-7}$ and $2{\cdot}423 \times 10^{-7}$ S. The difference in G_{in} and G_{morph} values indicates that there was a shunt at the soma and the magnitude of this varied between neurones. The shunt could be due either to a poor seal round the electrode or a lower R_m value at the soma. We can not distinguish between the two but a soma shunt would cause R_n and τ_0 to be underestimated, the effect being proportionally greater on R_n (see Gustafsson & Pinter, 1984). Therefore G_{in} would be greater than G_{morph}, precisely the situation here. Irrespective of the cause of the shunt, the implication of the above is that our values of R_m are underestimated and therefore the true values of L for individual cells (and dendrites) are shorter. Thus these motoneurones are even more electrically compact than our data would suggest.

DISCUSSION

The results of this study provide a quantitative description of both the general morphology and electrical geometry of jaw-elevator motoneurones and so provide a basis for comparing these motoneurones to others. One factor that becomes immediately evident in any such comparison is the relatively small size of elevator motoneurones compared to the more commonly studied cat spinal motoneurones. For example the mean soma diameter of elevator motoneurones is approximately half that of spinal motoneurones (Cameron *et al.* 1985; Rose *et al.* 1985; Cullheim *et al.* 1987), and their membrane area is approximately one third that of lumbosacral motoneurones (mean = $5{\cdot}58 \times 10^5$; Cullheim *et al.* 1987). The difference in areas can be attributed to the greater number of dendrites given off by spinal motoneurones (mean of 11·7; Cullheim *et al.* 1987) and the fact that on average the primary dendrites of spinal motoneurones have larger primary diameters (mean = 6·6 μm; Cullheim *et al.* 1987) than those of rat elevator motoneurones (mean = 4·3 μm) and so would be expected to result in dendritic trees of larger surface area (Ulfhake & Kellerth, 1981, 1983).

However, there are important differences in the pattern of branching, in particular the relative lengths of terminating dendritic branches. The terminating branches of spinal motoneurones have longer mean lengths than non-terminating branches (Rose *et al.* 1985; see also Fig. 1 of Cullheim *et al.* 1987) whereas the terminating dendrites of both elevator and abducens and laryngeal motoneurones (see Fig. 12 of Bras *et al.* 1987) are generally among the shortest dendritic segments. For example the length of terminating dendrites of hindlimb motoneurones can exceed the combined length of other dendritic segments along the same path length (see Fig. 1 of Cullheim *et al.* 1987). Terminating segments would have the smallest diameters and so for any given length would exert a much greater effect on the total electrotonic length of the dendrite. Therefore long distal dendrites will have a disproportionate effect on electrotonic length and would result in more attenuation of current in the distal portion of the dendritic tree. The result is that the distal dendrites of elevator motoneurones would contribute relatively less to the total electrotonic length of the dendrite than would be the case for spinal motoneurones.

Both Fleshman *et al.* (1988) and Clements & Redman (1989) have described for hindlimb motoneurones how the combined diameter of the dendritic tree varies with electrical distance from the soma. When R_m was assumed to be uniform throughout the neurone the combined diameter remained constant over the proximal 23% of the neurone and then tapered over the remaining part of the neurone (Clements & Redman, 1989). Fleshman *et al.* (1988) have calculated the profile of the equivalent cable assuming either a step-like or sigmoidal increase in R_m throughout the neurone. The result was that diameter remained constant over the proximal 30–35% of the dendritic tree and then tapered (inferred from Fig. 9 or Fleshman *et al.* 1988). Similar trends were seen in our data but with the difference that the combined diameter remained constant over a longer equivalent distance from the soma (about 50%).

In principle the reduction in diameter could be due to: (1) tapering of individual dendrites, either due to tapering in diameter between segments and/or early termination of branches, (2) individual dendrites not tapering but terminating at

different electrical lengths, and (3) tapering of individual dendrites combined with a difference in their electrical lengths. We were able to distinguish the cause of this tapering by showing that the individual dendrites approximated electrically to cylinders of constant diameter which terminated at different electrical lengths and so implying that the tapering of the combined dendritic tree could be ascribed to the second of the three possibilities outlined above. A similar analysis has not so far been reported for the hindlimb material and so the cause of the tapering of the combined dendritic tree remains to be made explicit. Clements & Redman (1989) stated that the tapering in the combined dendritic tree of spinal motoneurones could be ascribed to 'a combination of premature dendritic terminations and taper in the diameter of terminal dendrites (Ulfhake & Kellerth, 1981)'. However, they presented no specific evidence to justify this.

As individual dendrites of elevator motoneurones can be represented as cylinders current injection into these dendrites is more akin to injecting current off-centre into a cylinder of uniform diameter. An important practical result is that wide variations in the electrical lengths of individual dendrites will lead to errors in localizing synapses on dendrites (Redman & Walmsley, 1983). In consequence current flow in their dendrites must be simulated with a compartmental model and not by an equivalent cylinder model of constant taper.

Finally we have assumed in all our calculations that R_m is uniform throughout the neurone but there is increasing evidence that the soma and dendritic membranes may have different values of R_m (see discussion in Fleshman *et al.* 1988; Clements & Redman, 1989) and also that R_m may perhaps vary in a uniform manner throughout the dendritic tree (Fleshman *et al.* 1988; Clements & Redman, 1989). A lower R_m value at the soma than the dendrites may be of functional significance in that it would provide a means of reducing electrical interactions between dendrites as the soma would act as a shunt. Thus our suggestion is that elevator motoneurones may organize their electrical geometry so as to optimize current transfer from dendrites to soma and that this is enhanced by two adaptations. One is to ensure that the individual dendrites approximate electrically to uniform cables over most of their length. The result is that current flow to the soma will be optimal because the gradient of the electrotonic potential will remain constant throughout the length of the cylinder. The second and more speculative suggestion is that current flow to the soma is also favoured by a lower R_m at the soma than over the dendrites.

We are grateful to the Wellcome Trust for supporting this work. The data reported formed part of the PhD thesis of Jane A. Moore (University of Leeds).

REFERENCES

APPENTENG, K., DONGA, R. & WILLIAMS, R. G. (1985). Morphological and electrophysiological determination of the projections of jaw-elevator muscle spindle afferents in rats. *Journal of Physiology* **369**, 93–113.

APPENTENG, K. & GIRDLESTONE, D. (1987). Transneuronal transport of wheat germ agglutinin-conjugated horseradish peroxidase into trigeminal interneurones of the rat. *Journal of Comparative Neurology* **258**, 387–396.

APPENTENG, K. & MOORE, J. A. (1988). The electrical geometry of rat trigeminal motoneurones. *Journal of Physiology* **396**, 55*P*.

BLAKEMORE, C., JACK, J. J. B., LARKMAN, A. U. & MASON, A. (1987). Electrical geometry of spiny neurones in slices of cat and rat visual cortex studied using intracellular recording and horseradish peroxidase injection. *Journal of Physiology* **382**, 178*P*.

BLOOMFIELD, S. A., HAMOS, J. E. & SHERMAN, S. M. (1987). Passive cable properties and morphological correlates of neurones in the lateral geniculate nucleus of the cat. *Journal of Physiology* **383**, 653–692.

BRAS, H., GOGAN, P. & TYC-DUMONT, S. (1987). The dendrites of single brain-stem motoneurons intracellularly labelled with horseradish peroxidase in the cat. Morphological and electrophysiological differences. *Neuroscience* **22**, 947–970.

CAMERON, W. E., AVERILL, D. B. & BERGER, A. J. (1985). Quantitative analysis of the distribution of the dendrites of cat phrenic motoneurones stained intracellularly with horseradish peroxidase. *Journal of Comparative Neurology* **230**, 91–101.

CLEMENTS, J. D. & REDMAN, S. D. (1989). Cable properties of cat spinal motoneurones measured by combining voltage clamp, current clamp and intracellular staining. *Journal of Physiology* **409**, 63–87.

CULLHEIM, S., FLESHMAN, J. W., GLENN, L. L. & BURKE, R. E. (1987). Membrane area and dendritic structure in type-identified triceps surae alpha motoneurones. *Journal of Comparative Neurology* **255**, 68–81.

EGGER, M. D. & EGGER, L. D. (1982). Quantitative morphological analysis of spinal motoneurones. *Brain Research* **253**, 19–30.

FLESHMAN, J. W., SEGEV, I. & BURKE, R. E. (1988). Electrotonic architecture of type-identified α-motoneurones in the cat spinal cord. *Journal of Neurophysiology* **60**, 60–85.

GUSTAFSSON, B. & PINTER, M. J. (1984). Relations among passive electrical properties of lumbar α-motoneurones of the cat. *Journal of Physiology* **356**, 401–431.

JACK, J. J. B. (1979). An introduction to linear cable theory. In *The Neurosciences Fourth Study Program*, ed. SCHMITT, G. O. & WORDEN, F. G., pp. 324–337. MIT Press, Cambridge, MA, USA.

JACK, J. J. B. & REDMAN, S. (1971*a*). The propagation of transient potentials in some linear cable structures. *Journal of Physiology* **215**, 283–320.

JACK, J. J. B. & REDMAN, S. (1971*b*). An electrical description of the motoneurone and its application to the analysis of synaptic potentials. *Journal of Physiology* **215**, 321–352.

JANKOWSKA, E. (1985). Further indications for enhancement of retrograde transneuronal transport of WGA-HRP by synaptic activity. *Brain Research* **341**, 403–408.

MESULAM, M.-M. (1982). Principles of horseradish peroxidase neurochemistry and their applications for tracing neural pathways. In *Tracing Neural Connections with Horseradish Peroxidase*, ed. MESULAM, M.-M., pp. 1–151. John Wiley and Sons, New York, London.

MOORE, J. A. & APPENTENG, K. (1990). The membrane properties and firing characteristics of rat jaw-elevator motoneurones. *Journal of Physiology* **423**, 137–153.

RALL, W. (1959). Branching dendritic trees and motoneurone resistivity. *Experimental Neurology* **1**, 491–527.

RALL, W. (1962). Theory of physiological properties of dendrites. *Annals of the New York Academy of Sciences* **96**, 1071–1092.

RALL, W. (1977). Core conductor theory and cable properties of neurons. In *Handbook of Physiology, The Nervous System*, ed. BROOKHART, J. M. & MOUNTCASTLE, V. B., pp. 39–97. American Physiological Society, Bethesda, MD, USA.

RALL, W., BURKE, R. E., SMITH, T. G., NELSON, P. G. & FRANK, K. (1967). Dendritic location of synapses and possible mechanisms for the monosynaptic EPSP in motoneurones. *Journal of Neurophysiology* **30**, 1169–1193.

REDMAN, S. J. & WALMSLEY, B. (1983). The time course of synaptic potentials evoked in cat spinal motoneurones at identified group Ia synapses. *Journal of Physiology* **343**, 117–133.

ROKX, J. T. M., VAN WILLIGEN, J. D. & JUCH, P. J. W. (1985). Distribution of innervating neurons of masticatory muscle spindles in the rat; an HRP study. *Experimental Neurology* **88**, 562–570.

ROSE, P. K., KEIRSTEAD, S. A. & VANNER, S. J. (1985). A quantitative analysis of the geometry of cat motoneurones innervating neck and shoulder muscles. *Journal of Comparative Neurology* **239**, 89–107.

SCHIERWAGEN, A. & GRANTYN, R. (1986). Quantitative morphological analysis of deep superior colliculus neurons stained intracellularly with HRP in the cat. *Journal für Hirnforschung* **27**, 611–624.

TURNER, D. A. & SCHWARTZKROIN, P. A. (1980). Steady-state electrotonic analysis of intracellular stained hippocampal neurons. *Journal of Neurophysiology* **44**, 184–199.

TURNER, D. A. & SCHWARTZKROIN, P. A. (1983). Electrical characteristics of dendrites and dendritic spines in intracellularly-stained CA3 and dentate hippocampal neurons. *Journal of Neuroscience* **3**, 2381–2394.

ULFHAKE, B. & KELLERTH, J.-O. (1981). A quantitative light microscopic study of the dendrites of cat spinal α-motoneurones after intracellular staining with horseradish peroxidase. *Journal of Comparative Neurology* **2020**, 571–583.

ULFHAKE, B. & KELLERTH, J.-O. (1983). A quantitative morphological study of HRP labelled cat α-motoneurones supply different hindlimb muscles. *Brain Research* **264**, 1–19.

YOSHIDA, A., TSURU, K., MITSUHIRO, Y., OTANI, K. & SHIGENAGA, Y. (1987). Morphology of masticatory motoneurons stained intracellularly with horseradish peroxidase. *Brain Research* **416**, 393–401.